analytical chemistry

pubs.acs.org/ac Article

Rock-to-Pharma: Characterization of Shale Oil-Based Nonbiological Complex Drugs along the Production Process by High-Resolution Mass Spectrometry

Ole Tiemann, Christopher P. Rüger,* Lukas Schwalb, Martha L. Chacón-Patiño, Thomas Gröger, and Ralf Zimmermann

Cite This: *Anal. Chem.* 2024, 96, 13050−13060 Read Online

ACCESS | Metrics & More | Article Recommendations | Supporting Information

ABSTRACT: Antibiotic resistance has become a primary concern in medicine because of the overuse and misuse of classical pharmaceuticals. Recently, nonbiological complex drugs (NBCDs) have gained interest for their complex pharmacological profiles. Bituminosulfonates, which have lately been tentatively allocated toward NBCDs, are pharmacologically well-studied and show low potential in resistance development. However, molecular composition knowledge is limited. With this work, we present a comprehensive approach to investigate the manufacturing process of complex pharmaceuticals like bituminosulfonates on a molecular level via Fourier-transform ion cyclotron resonance mass spectrometry. The application of various hyphenations and ionization techniques comprehensively covers the entire mass and polarity range of the matrix, and the high sensitivity enables the identification of significant and minor chemical alterations caused by the multistep manufacturing process. The distillation of the shale crude oil eliminates highly aromatic PAH and PASH constituents. ESI(−) revealed strong PAH- and PASH-sulfonate formation after reacting the shale oil distillate with sulfuric acid. Increasing alkylation reduced the sulfonation yield, instead causing oligomerization side reactions, as observed by APPI analysis. Furthermore, multidimensional gas chromatography coupled with high-resolution mass spectrometry verified core structural motifs. With this work, we demonstrate the high potential of FT-ICR MS in NBCD process analysis. The results also give valuable information for future pharmacological investigations focusing on specific compound classes or properties.

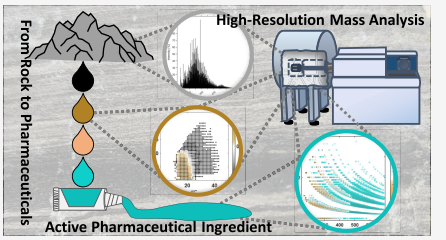

1. INTRODUCTION

In the past decades, antibiotic resistance has become a primary concern in medicine.[1−3] The over- and misuse of pharmaceuticals has led to the emergence of resistant bacteria.[1] This development poses a significant threat to public health, and the development of new antibiotics has slowed down, further exacerbating the problem. Classical antibiotic pharmaceuticals, such as penicillin[2] and aminoglycoside formulations,[3] are simple mixtures with well-defined active pharmaceutical ingredients (APIs). Established analytical workflows for these polar compounds feature primarily high-performance liquid chromatography (HPLC) with UV spectroscopic or triple quadrupole mass spectrometric detection (QqQ-MS).[4−7]

However, recently, medicinal products called "nonbiological complex drugs" (NBCDs) have gained medicinal, regulatory, and economic interest for their complex pharmacological profiles and low potential for resistance development.[8−10] They are defined as medicinal products where the API is neither a homomolecular structure nor a biological medicine.[10] Crommelin et al.[8] added to the nature of NBCDs that they "cannot be isolated and fully quantitated, characterized, and described by physicochemical analytical means" referring to the analytical methods in the *Pharmacopeia*. Therefore, NBCDs are defined by their manufacturing process and bulk parameters, whereas the composition, quality, and in vivo performance of NBCDs are highly dependent on the manufacturing process of both the API and the formulation.[11] Classic examples with broad coverage of induced health effects are liposomes,[12] iron-carbohydrate drugs,[13] or glatiramoids.[14] Also, bituminosulfonate formulations have been tentatively allocated toward NBCDs,[15] featuring broad and valuable antibiotic effects, among other properties. Furthermore, bituminosulfonates were found to show a low potential for resistance development.[16−18] These APIs are derived from kerogen-containing rocks, which are subjected to a dry distillation process to obtain sulfur-rich shale oil.[15,19] The key to receiving the final API is a vacuum distillation followed by sulfonation. Depending on the exact production pathway, sodium hydroxide or ammonia is used for neutralization, receiving sodium bituminosulfonates (SBS) or ammonium

Received: March 8, 2024
Revised: June 28, 2024
Accepted: July 2, 2024
Published: July 31, 2024

Downloaded via FLORIDA STATE UNIV on September 4, 2024 at 19:11:10 (UTC).
See https://pubs.acs.org/sharingguidelines for options on how to legitimately share published articles.

ACS Publications © 2024 American Chemical Society

https://doi.org/10.1021/acs.analchem.4c01288
Anal. Chem. 2024, 96, 13050−13060

bituminosulfonates (ABS), respectively. The use and efficacy as a therapeutic agent have been documented since 1882.[19] Interestingly, a low potential for antimicrobial resistances in bacterial cells has been found,[20−22] and the exact pharmaceutical mechanisms are currently being investigated.[18]

While the pharmaceutical effects are well-documented for SBS[21] and ABS,[16,20] molecular composition knowledge is limited.[15] However, chemical speciation along the different processing steps is crucial for understanding transformation processes and ensuring high-quality standards. Previous studies were able to identify alkylated thiophenes and benzothiophenes in the precursor distillates[23,24] and sulfonated alkylbenzenes, -thiophenes, and other sulfonated arenes in the APIs.[15,25] Challengingly, analytical methodologies for targeting aromatic sulfonates are rarely found in the literature,[26,27] and regulatory solutions for in-depth speciation are entirely missing. Standard spectroscopic techniques are not able to cope with the tremendous complexity and could only be suitable for high-throughput quality control and bulk analysis.[28,29] Molecular information can be gained by high-performance chromatography combined with mass spectrometry.[28,30] However, the development of chromatographic protocols can be tedious[31] and error-prone. Unlike chromatography, most atmospheric pressure ionization techniques are directly applicable with minimal to no sample preparation.[31] Thus, direct mass spectrometry with atmospheric pressure ionization has become increasingly popular in pharmaceutical research lately.[32] High-field Fourier-transform ion cyclotron resonance mass spectrometry (FT-ICR MS) has been successfully deployed for in-depth molecular speciation of dissolved organic matter,[33] fossil fuels,[34] proteins, as well as other complex organic mixtures.[35] The lowest mass measurement error (root-mean-square error, RMSE, below 40 ppb), highest dynamic range of any mass analyzer, and automatic gain control (AGC)[36] minimizing scan-to-scan variations in ion number enable the identification of species that differ in less of the mass of an electron.[37]

This study aims to present the analytical potential of ultrahigh-resolution mass spectrometry for the molecular-level description of NBCDs. Bituminosulfonate formulations and their multistep production process are complex examples of the importance of real-world antibiotics. Recently, we have successfully shown the potential of comprehensive gas chromatography (GCxGC) with high-resolution time-of-flight mass spectrometry (HR-ToF-MS) for unraveling the lighter SBS fraction, featuring lower molecular weight constituents.[15] However, gas chromatography reaches its instrumental limits for higher molecular weight NBCDs, such as ABS.[31] Direct injection mass spectrometry may overcome these limitations and enable immediate complex mixture analysis. However, as the molecular formulas attribution relies on resolving isobaric constituents without chromatography, particularly heteroelements can be problematic.[38,39] Here, we show that the increased sulfur content with over 10 wt %, given by the formulation, frequently causes mass splits below 1 mDa caused by the combination with additional heteroatoms. Moreover, the different processing steps are used for in-depth discussion on chemical changes during the manufacturing process utilizing chemical fingerprint visualization, e.g., modified van Krevelen (S/C) and double-bond-equivalent versus carbon number (DBE vs #C) diagrams, as well as fold-change (FC) analysis. Combining electrospray analysis in negative (ESI(−)) and positive modes (ESI(+)), as well as atmospheric pressure photoionization (APPI), allows to cover a wide chemical space, ensuring untargeted explorative MS analysis in a pharmaceutical context.

2. MATERIAL AND METHOD

2.1. Material. Ammonium bituminosulfonates (ABS, e.g., Ichthammol (EC#: 232-439-0), Ichthyol (EC#: 232-439-0)) and the nonsulfonated starting materials "vacuum distillate (shale oil), middle" (VDM, EC#: 269-646-0) as well as "shale crude oil" (SCO, EC#: 269-646-0) and the bituminous schist (BS) source rock with maritime origin analyzed within this study originate from the same production process and were provided by Ichthyol-Gesellschaft Cordes, Hermanni & Co. (GmbH & Co.) KG, Hamburg, Germany. The schematic description of the manufacturing process relevant for this paper is given in Figure 1. A detailed scheme of the complete manufacturing process is given in Figure S1.

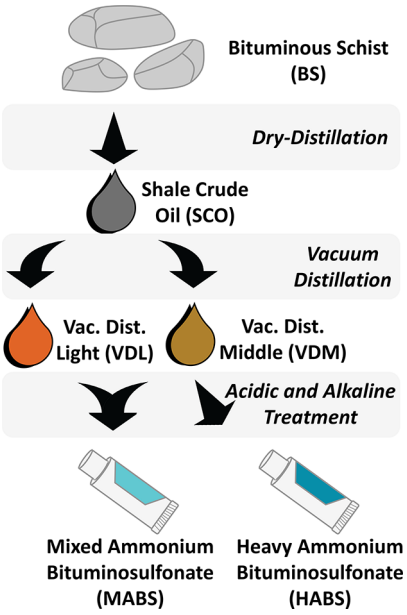

Figure 1. Flowchart of the manufacturing process of ammonium bituminosulfonate (ABS). Mixed ABS (MABS) refers to the product manufactured from a combination of the vacuum distillate light and the vacuum distillate middle (VDM), while heavy ABS (HABS) is manufactured exclusively from VDM.

2.2. Method. *2.2.1. Thermogravimetry Fourier-Transform Ion Cyclotron Resonance Mass Spectrometry with Atmospheric Pressure Photoionization (TG APPI FT-ICR MS).* Prior to analysis, the BS was homogenized with a 6750 Freezer/Mill (SPEX CertiPrep Inc., Metuchen, NJ, USA). The homogenized BS was then measured by thermogravimetry (TG) coupled to APPI FT-ICR MS. The detailed setup can be found elsewhere.[40−43] Thermal analysis was performed with a thermobalance (TG 209, Netzsch Gerätebau, Selb Germany) hyphenated to a modified GC-APCI II ion source (Bruker Daltonics, Bremen Germany). In addition, BS was also analyzed with a second thermobalance (STA 449F3, Netzsch Gerätebau, Selb Germany) using a ceramics crucible with pinhole for more accurate mass loss information.

The temperature programs are shown in Table S1. Evolved gases were transferred into the mass spectrometric ion source via an interface and a transfer line, which were operated at 280

https://doi.org/10.1021/acs.analchem.4c01288
Anal. Chem. 2024, 96, 13050−13060

°C. Time-resolved mass spectrometric detection was carried out with a Bruker Apex II ultra FT-ICR MS (Bruker Daltonics, Bremen, Germany) equipped with a 7 T superconducting magnet recording from m/z 100 to 1000 with a 2 s transient (4 Megawords, 10 μscans) and a resulting resolving power of 260 000 at m/z 400. Comprehensive time-resolved processing and internal quadratic precalibration on homologue rows were performed with Data Analysis 5.1 (Bruker Daltonics, Bremen, Germany). The time-resolved data were exported by Visual Basic scripting with S/N 9. Further data treatment was done in CERES, a self-written program based on in-house MATLAB scripting (MATLAB R2020b) for further processing by feature detection and sum formula calculation. Additionally, every single mass spectrum was recalibrated to correct for frequency shifts resulting from varying ion loads in the FT-ICR MS cell.[44] #C 2−100, #H 2−200, #N 0−1, #O 0−4, #S 0−4, H/C 0.4−2.4, DBE 0−30, and sum formula error of 1 ppm were set as sum formula attribution restrictions.

2.2.2. Direct Infusion ESI(±) and APPI FT-ICR MS. For negative/positive-ion micro-ESI, samples were dissolved in 1:1 toluene:methanol (v/v) at a concentration of 50 μg/mL. Samples were directly infused into a custom-built micro-ESI source at 0.55 μL/min and ionized with a needle voltage of −2.8 kV for negative-ion and 3.2 kV for positive-ion. Analyses were performed by adding tetramethylammonium hydroxide (TMAH, 0.005% v/v) to the sample solutions to promote deprotonation (negative-ion) and formic acid 1% v/v to promote protonation (positive-ion). For APPI(+), samples were diluted in 1:1 toluene:methanol (v/v) to a concentration of 25 μg/mL and directly infused at 50 μL/min into an APPI Ion Max source (Thermo-Fisher Scientific, Inc., San Jose, CA, U.S.A.), operated with a vaporizer temperature of 320 °C. For APPI, N_2 sheath gas was used at 50 psi and N_2 auxiliary gas at 32 mL/min. Gas-phase neutrals were photoionized by a 10/10.6 eV ultraviolet krypton lamp (Syagen Technology, Inc., Tustin, CA, U.S.A.). Ions were analyzed with a custom-built 21T FT-ICR mass spectrometer.[45] For analyses, 1.5×10^6 charges were accumulated in an external multipole ion trap and subsequently transferred to the ICR cell, as a function of m/z, by a decreasing auxiliary radio frequency. Excitation and detection were carried out on the same pair of the dynamically harmonized ICR electrodes, maintained at 6 V trapping potential. Time-domain transients of 3.2 s were collected with Predator Software, and at least, 100 time-domain transients were averaged for all the samples. Mass spectra were phase-corrected and internally calibrated with sulfur- and oxygen-containing homologous series using the "walking" calibration method,[46] followed by mass list export with S/N 6, resulting in a resolving power of R > 3,000,000 at m/z 400 for all ionization techniques. Finally, the mass lists were further processed with a home-built software named CERES (MATLAB R2020b) for sum formula assignment. The sum formula attribution restrictions were set to #C 2−100, #H 2−200, #N 0−1, #O 0−10, #S 0−6, H/C 0.4−2.4, DBE 0−25 for ESI(−) and to #C 2−100, #H 2−200, #N 0−3, #O 0−10, #S 0−6, #Na 0−1, H/C 0.4−2.4, DBE 0−25 for ESI(+) and APPI. The sum formula error limit was set to 150 ppb, and sum formulas could generally be obtained with a root-mean square error below 30 ppb for ESI(−) and APPI measurements and below 50 ppb for ESI(+) analyses.

2.2.3. Comprehensive Two-Dimensional Gas Chromatography Coupled to Electron Ionization High-Resolution Time-of-Flight Mass Spectrometry (GCxGC EI HR-ToF-MS). The GC × GC measurements were carried out on a Pegasus GC-HRT 4D (LECO, St. Joseph, USA).[15,31] In summary, a 60 m BP1 (0.25 mm internal diameter, 0.25 μm film thickness, SGE) column was used in the first dimension and 1.5 m BPX50 (0.1 mm internal diameter, 0.1 μm film thickness, SGE) in the second dimension. Before the measurement, the APIs were mixed with tetramethylammonium hydroxide (1:2 w/v) and diluted 1:10 with a mixture of water/methanol (1:1 v/v). 0.5 μL of the solution was injected at 350 °C with a split of 1:10. The oven program started at 40 °C with a heat rate of 10 °C/min up to 120 °C and decreased to 1 °C/min until the oven reached the end temperature of 320 °C. For the shale oil and distillates, 1 μL of the samples were injected at 350 °C with a split of 1:200. The oven program starts at 70 °C, keeps the temperature for 5 min, heats up at 1 °C/min up to 320 °C, and keeps the temperature for 10 min. For both methods, the offset of the second oven was set to 30 °C relative to the first oven and the offset of the modulator was set to 15 °C relative to the second oven. The ions were acquired between m/z 15 and 500 with an acquisition rate of 100 Hz. Perfluorotributylamine was used for internal mass calibration. A mass resolution of at least ≥25 k for m/z 218.9856 with a mass error below 1 ppm was achieved. Acquired mass spectra were calibrated and processed with the ChromaTOF HRT software (v5.10, LECO, St. Joseph, USA).

3. RESULTS AND DISCUSSION

3.1. Thermal Analysis of the Source Rock. To mimic the first step of the API production, an aliquot of the homogenized BS was investigated by straight TG analysis. Further chemical insights of the evolved gas phase were achieved by TG APPI FT-ICR MS analyzes. As the BS is smoldered at 450 °C on an industrial scale, aside from a common linear gradient temperature protocol (TP1), a temperature program with constant step at 450 °C for 30 min (TP2) has been measured. Analysis deploying a linear gradient and a crucible with pinhole (common for studying distillation behavior) shows a distinct mass loss step between 340 and 520 °C with a maximum at 430 °C and a mass loss of about 10% (Figure 2). This process fits typical pyrolysis temperatures and can be attributed to the smoldering-induced pyrolysis of the BS. Furthermore, the observations match the stable temperature of the dry distillation on a large industrial scale as well as the mass loss found for TP2. For TP2, mimicking the real-world process, after approximately 15−20 min, no mass loss was observed anymore. This finding suggests a pronounced pyrolysis of the organic material in the API educt BS and even exceeds the manufacturers' specifications.

Mass spectrometric investigation of the evolved gas from TP2 revealed significant amounts of sulfur-containing compounds (SCCs) attributing 80% of the overall mass spectrometric abundance (Figure S2). The overall chemical characteristic is dominated by alkylated homologue series of aromatic core structural moieties and reassembles common petroleum distinctive features. In contrast to our previous thermal analysis mass spectrometry work on petroleum matrices,[40,42] compounds with a higher number of sulfur are dominant in this matrix, with the CHS_1 and CHS_2 classes being the most abundant. According to the literature, SCCs like thiophenes and benzothiophenes are emitted within a temperature range of about 360−540 °C with short-chain alkyl thiophenes and benzothiophenes being emitted at around 460 °C and long-chain alkyl thiophenes being emitted at

https://doi.org/10.1021/acs.analchem.4c01288
Anal. Chem. 2024, 96, 13050−13060

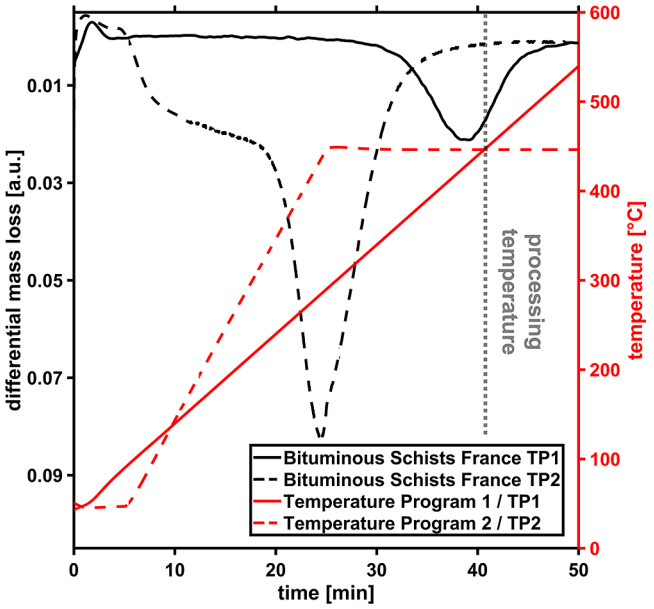

Figure 2. Differential mass loss curves for the thermogravimetric analysis of the bituminous schists source rock from France with two temperature programs (TP1/TP2, see Table S1) with a linear gradient up to 600 °C and with a constant step at 450 °C, mimicking the oven smoldering temperature in the production process.

temperatures above 500 °C.[47] Evolved gas analysis with high-resolution mass spectrometry can successfully track and resolve this chemical complexity (Figures S3 and S4). The time-resolved mass spectrometric analysis shows two evolving events (Figure S3), which can be separated into a desorption step (T < 300 °C) and a pyrolysis step (T > 300 °C). In accordance with the literature, the m/z ratio increases with increasing temperature, resulting in compounds with higher aromaticity and longer alkyl side chains. During the pyrolysis, a broad mass range is detected covering the full desorption range, while simultaneously showing a shift toward slightly higher masses as well as higher intensities in the higher mass ranges. Comparing these mass spectrometric data to the time-resolved differential mass loss (Figure 2), it was found that the most abundant mass loss was detected toward the end of the pyrolysis phase, while the mass spectrometric data indicate a more constant mass loss. It is expected that during the pyrolysis phase, inorganic gases like sulfur dioxide and carbon dioxide are also emitted among the detected organic substances. Also, Guo et al.[48] have shown the potential of sulfur-containing marine natural products for drug discovery and drug development. As the investigated BS was found to have a marine origin and similar SCC moieties, this further highlights the pharmacological potential of this matrix. Even though the production process of the API involves a pharmacologically uncommon thermal processing step, high-resolution mass spectrometric analysis can address this production step by thermal analysis coupling. However, a gas-phase ionization technique, such as APPI, was needed, and routine electrospray ionization would not be applicable. Sampling of the evolved gas mixture also allowed us to trace more polar heteroatom-containing polyaromatic species, which we have seen before in studies on fossil samples.[40,42] Thus, thermogravimetry with mass spectrometric evolved gas analysis aids in process understanding and sets the basis for further investigations on the respective shale crude oil, distillate, and sulfonated API products.

3.2. Characterization of the Shale Crude Oil and Its Resulting Vacuum Distillate. Mass spectrometric insights into the evolved gas mixture released during thermal analysis highlight a high contribution of SCCs, such as polycyclic aromatic sulfur heterocycles (PASHs). Species with up to three sulfur atoms have been attributed. Hence, the spectral complexity is strongly affected by the sulfur split (C_3 versus SH_4, 3.4 mDa), commonly reported in *Petroleomics* for fossil matrices. With lower abundance, other compound classes containing nitrogen and oxygen functionalities have also been observed (Figure S2), resulting in a high isobaric complexity. However, thermal analysis with a slow pyrolysis temperature profile may simplify the detected complexity of the evolved gas mixture at a given time. On the contrary, typical direct infusion "dilute and shoot" analysis must cope with the full isobaric complexity of the SCO resulting from the source rock pyrolysis and its manufacturing product VDM. Consequently, an ultrahigh-field 21 T FT-ICR MS facility (21 T FT-ICR MS platform at the National High Magnetic Field Laboratory, NHMFL) was utilized to ensure the highest available mass spectrometric performance.[45]

Direct infusion analysis of the condensed shale oil as well as the first production step deploying vacuum distillation could successfully address the tremendous isobaric complexity, TGA FT-MS has already illustrated. Thereby, 7207 and 4635 molecular formulas could be attributed for the SCO and distillate, reflecting the significant decrease in complexity, respectively. Ultrahigh-resolution mass spectrometric analysis revealed baseline-resolved sub-mDa mass splits, with the most challenging being given by a combination of sulfur, oxygen, and nitrogen heteroatoms ($\Delta m/z$ 0.69 mDa for C_6N vs H_6O_3S, Figure S5). This mostly low-intense mass split requires high sensitivity, a mass resolving power of at least 580,000 at m/z 400, and ppb-level mass accuracy for baseline resolving and confidently attributing the two components. This clearly points out the need of FT-ICR MS performance for in-depth molecular description. Calculating the intensity-weighted relative elemental composition of the matrices directly gives first insights into the high heteroatom content (Figure S8). Depicting the assigned sum formulas into compound classes enables the identification of compound class-specific distillation-related tendencies (Figure 3). Therefore, constituents with the same number of heteroatoms, e.g., pure hydrocarbons, are summarized in the CH class, while compounds that include organically bound sulfur atoms are grouped in the S_x classes. According to the analysis of the source rock, over 80% of the overall abundance was assigned toward SCCs for both, the SCO and vacuum distillate VDM. More than 60% of these compounds belong to the S_1 and S_2 classes, resulting in a significantly higher sulfur content than that found in the other shale oils.[49] However, the general molecular distribution reassembles petroleum characteristics and follows the Boduszynski continuum with superimposed homologue alkylation rows spanning from m/z 150 to 650 in the SCO.[50]

By distillation, all compound classes showed significant decreases in assigned sum formulas of at least 20%, pointing out a significant reduction of the chemical complexity by the initial GMP-regulated processing step of the SCO toward the API matrices. The distillate process affected mostly classes with multiple sulfur atoms, whereas a relative enrichment of S- and SO-classes could be found. As shown in Figure 3A, S_1-

https://doi.org/10.1021/acs.analchem.4c01288
Anal. Chem. 2024, 96, 13050−13060

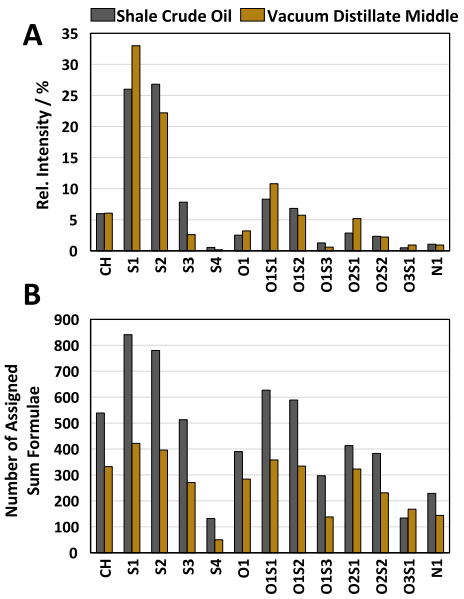

Figure 3. Compound class distribution for the direct infusion APPI FT-ICR MS measurements of the raw shale crude oil (gray) and the vacuum distillate middle (VDM, brown) based on (A) relative summed intensity and (B) number of assigned sum formulas.

containing compounds (e.g., S_1 and O_1S_1) are relatively enriched in the distillate, whereas constituents with higher sulfur contents are clearly depleted. We hypothesize that this finding is due to characteristic shifts in vapor pressure and boiling point with adding heteroatoms to the polyaromatic skeleton.

Complementary to the FT-ICR MS analysis, group-type analysis of the GCxGC EI-HR-ToF-MS results allowed for structural elucidation on these SCCs. The choice of column compositions ensures separation according to size and alkylation along the first chromatographic dimension, while separation according to aromaticity takes place along the second chromatographic dimension (Figures S6 and S7). EI leads to further structural information due to ionization technique-based fragmentation. Combining the chromatographic and mass spectrometric information enables the empiric definition of elution windows for distinct sum formulas, allowing a less time-consuming data evaluation (Figure S7). Thereby, thiophenes and benzothiophenes are most abundant before and after distillation. Additionally, sulfoxides and thioles have been identified, among other species. These sulfur-based functionalities were found to play an essential role in drug discovery and development, addressing different pharmaceutical issues depending on the sulfur moiety.[48,51] Therefore, the rich content in organic-bound sulfur sets high potential of the SCO and VDM for further processing from a pharmaceutical point of view.

Generally, the distillation process causes a decrease in average m/z and DBE for all compound classes (Figure S8) in the VDM. FT-MS analysis exposed that constituents containing no sulfur, such as CH, N_1 and O_1 class compounds, have been found with the same relative abundance before and after the distillation process. The CH class revealed lighter compounds with a significantly lower average m/z (Figure S9A) than the other compound classes. Considering the medium DBE prior distillation (DBE 10, 3-ring aromatics), a stable relative contribution can be explained after thermal separation. For the more polar compounds, such as N_1 and O_1 class species, low average m/z and relatively high mean DBE values prior to distillation could be found. We hypothesize that the lower mass has a stronger effect on the distillation behavior than the hydrogen deficiency (DBE), causing an overall stable relative proportion of these classes before and after distillation. This finding is in good agreement with the Boduszynski concept.[52−54]

Group-type GCxGC analysis of the 10 most abundant functionalities (Figure S9C) revealed that besides aromatic constituents, aliphatic and nonaromatic compounds are also present in the SCO and VDM. The majority of these compounds are fully saturated and therefore unsuitable for sulfonation.[27] However, these compounds have already been cut off to a large extent in a lighter distillation cut, not studied herein and investigated elsewhere.[15] For the VDM investigated in this study, complementary GCxGC analysis pointed out a low contribution of species with m/z below 150, mainly with DBE below 4, complementing the FT-ICR MS findings and simultaneously showing the applicability of FT-ICR MS as analytical conception for tracing the processing steps of medium- and heavy-weight compounds.

Both the FT-ICR MS and the GCxGC results show a clear gain in abundance for mono- and binuclear PASHs (e.g., thiophenes and benzothiophenes), as well as for two- and three-ring PAHs (e.g., naphthalenes and phenanthrenes). In contrast, higher aromatic compounds (DBE > 10) were drastically reduced by distillation, resulting in hardly any detection of core structural motifs larger than three-ring aromatics (Figure 4). For both, SCO and VDM, a uniform DBE distribution has been found for the CH class with a maximum at DBE 8 (biphenyls, Figure S10A/E). In contrast,

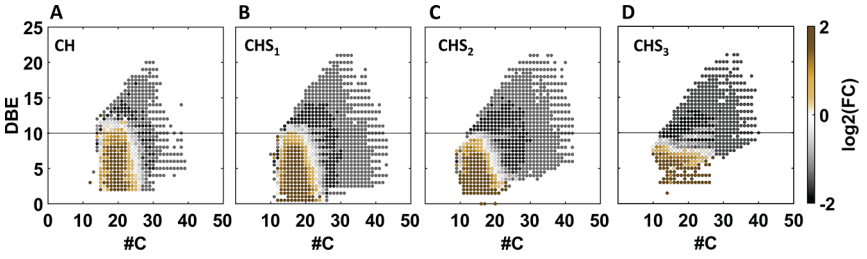

Figure 4. Double-bond equivalent vs carbon number (DBE vs #C) plots of APPI FT-ICR MS analysis of the shale crude oil and its resulting vacuum distillate illustrating the CH class (A), the CHS_1 class (B), the CHS_2 class (C), and the CHS_3 class (D). Color coding corresponds to the fold change (FC) based on the absolute abundance ratio of the compounds. Positive values account for an enrichment after distillation, while negative values point out depleted compounds after distillation. For orientation, a horizontal line was added at DBE 10. A clear distillation effect can be observed for all classes, causing lower DBE and m/z for the condensate.

https://doi.org/10.1021/acs.analchem.4c01288
Anal. Chem. 2024, 96, 13050−13060

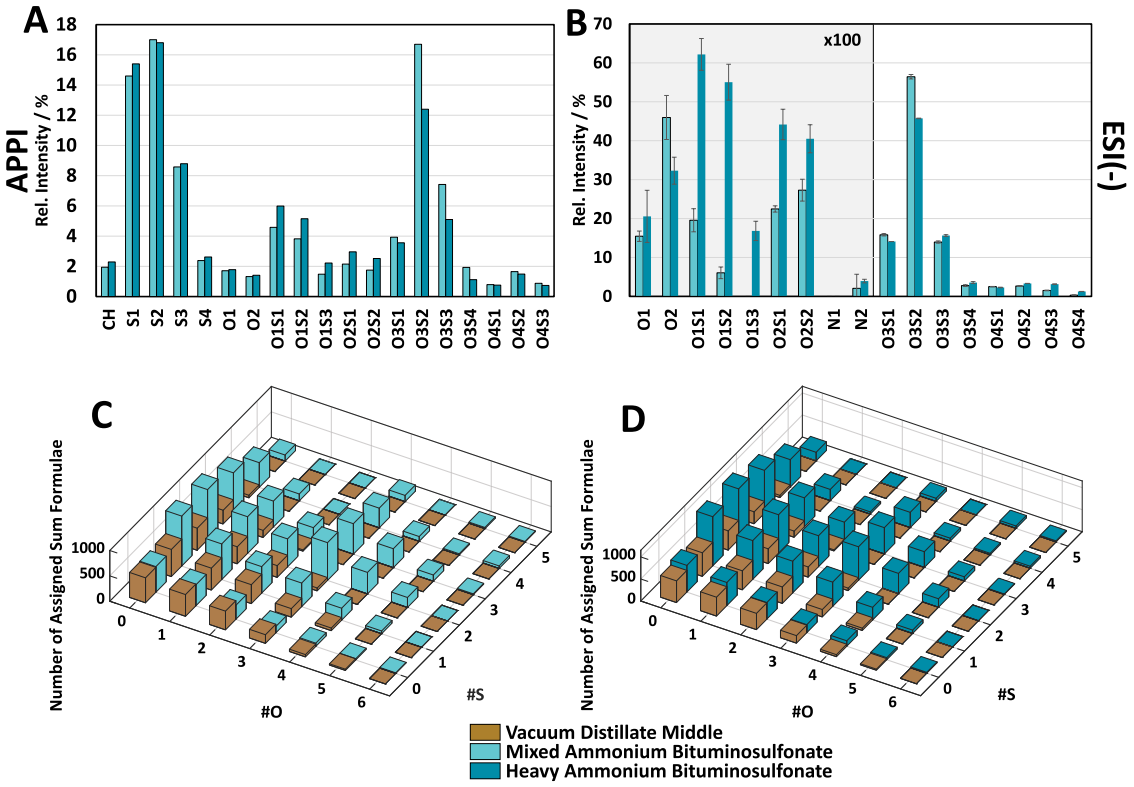

Figure 5. Compound class distribution for the direct infusion FT-ICR MS measurements of the mixed (MABS) and heavy ammonium bituminosulfonate (HABS) based on (A) relative summed intensity for APPI and (B) relative summed intensity for ESI(−). Due to low intensities, several compound classes were magnified 100-fold. (C) and (D) illustrate the number of assigned sum formulas in APPI resolved by their sulfur and oxygen content, comparing MABS to vacuum distillate middle (VDM) (C) and HABS to VDM (D), respectively.

characteristic DBE values were identified for the S_x classes (SCCs), belonging to thiophene-based core structures (Figure S10). This finding resulted by the thermodynamic stability in oil-formation, maturation, and exploration and is commonly reported in fossil matrices of various origins.[55] Furthermore, these compounds are less alkylated after distillation, reducing the risk of steric hindrance in subsequent steps of the process. Thiophanic, thiolic, or thioether-based SCCs, which are not suitable for sulfonation reactions,[27] were found to be significantly less present.

As shown, FT-ICR MS is applicable for the in-depth chemical description of these fossils and relatively low polar matrices as well as their compositional changes caused by the physicochemical processing. However, to obtain the API, the shale oil-based starting material is chemically altered by reacting with concentrated acids and bases. The combination of different ionization techniques becomes necessary to describe these highly polar matrices and the mechanisms causing the chemical modifications.

3.3. Chemical Description of the Ammonium Bituminosulfonates. To obtain the API, the shale oil-based raw material first reacts with concentrated sulfuric acid, causing a sulfonation reaction[56,57] before the mixture is neutralized with ammonia. Sulfonation ($+SO_3$, $+m/z$ 80) causes a substantial increase in polarity by adding one or several polar functionalities to the low polar aromatic cores[56], making ESI particularly suitable as an ionization method.[27] However, information about the sulfonation yield is limited. Furthermore, the temperature is monitored during the acidic and basic treatments but not actively controlled. Therefore, side reactions, such as oligomerization and oxidation, may also occur, making complementary APPI particularly necessary for targeting low and nonpolar species (Figures S17 and S18). Since both the mixed ammonium bituminosulfonate (MABS, Ichthammol) and the heavy ammonium bituminosulfonate (HABS, Ichthyol) are used as APIs, their detailed chemical characterization is crucial. The high isobaric complexity of the vacuum distillate precursor matrix as well as the vast variety of potential reaction pathways given by the acidic and basic treatments indicate the need to deploy different ionization approaches (APPI, ESI) for direct infusion FT-ICR MS analysis to comprehensively describe the isobaric complexity of these APIs, exemplarily given for an APPI FT-ICR MS analysis of HABS in Figure S11.

The intensity-weighted elemental compositions of SCO, VDM, MABS, and HABS show relatively strong alterations in the elemental composition and are displayed in Figure S8 for each direct infusion ionization technique. Comparing the number of assigned sum formulas prior and after the acidic and basic treatments (Figure S12A) highlights strong chemical alteration as expected, since the number of assigned sum formulas increases by a factor of 3 for the APPI analyses after the chemical treatment. Simultaneously, as shown in Figure S12B, each ionization technique used in this work found a reasonable number of assigned sum formulas uniquely being assigned by the certain ionization technique, further proving the need for this comprehensive approach. The most intense compounds identified by the APPI in the mixed (MABS) and heavy sulfonate (HABS) were found within the same mass range as the compounds identified in the vacuum distillate (VDM), ranging up to m/z 300. However, the general mass distribution of MABS and HABS also shows substantial

https://doi.org/10.1021/acs.analchem.4c01288
Anal. Chem. 2024, 96, 13050−13060

abundances up to m/z 700, resulting in higher average molecular masses (Figure S13A) and mean DBE values (Figure S13B) than in the precursor distillate and, thus, significant chemical alterations, as shown in Figure 5A/B. Furthermore, the chemical reaction process changes the carbon number and DBE distribution, resulting in a bimodal carbon number distribution (Figure S13A−C) and higher DBE values (Figure S13M−O) for the bituminosulfonates. Compounds belonging to the second part of the bimodal distribution with high carbon number and DBE are not observed for the distillate. Thus, we hypothesize that these heavier and more aromatic compounds are caused by oligomerization side reactions, e.g., due to cationic polymerization. The exothermic reaction with sulfuric acid drastically increases the reaction vessel temperature, making the generation of these side reaction products plausible. Unexpectedly, nitrogen-containing compounds neither altered in their number nor in their chemical composition, making them neutral process trace constituents. Notably, sulfur- and oxygen-containing compounds altered significantly, shifting toward higher sulfur and oxygen contents. The distillate shows a monomodal sulfur distribution and steadily declining oxygen distribution with increasing oxygen number (Figure 5C/D). After reaction with sulfuric acid, the bituminosulfonate products exhibit an increase in sulfur content (average #S increase of 0.69 from VDM to MABS and 0.63 from VDM to HABS) and in oxygen number (average #O increase of 0.91 from VDM to MABS and 0.75 from VDM to HABS).

The oxygen number distribution is showing a distinct maximum at three oxygen atoms per molecule. Molecular attribution and compound class grouping, given by the superior performance of the FT-ICR MS, allow to trace global reaction schemes.[42] In the here presented case, reaction with sulfuric acid should dominantly result in sulfonation ($+n(SO_3)$). For this purpose, Figure 5C/D combines the sulfur and oxygen distribution in a three-dimensional representation. A homogeneously declining hyper surface for increasing sulfur and oxygen is found for the distillate, whereas for both bituminosulfonates, two distinct maxima are observable. On the one hand, compounds low in oxygen (#O < 3) may be attributed to nonsulfonated compounds, predominantly consisting of highly alkylated unsaturated monomeric and oligomeric constituents, such as PASHs, thioethers, or sulfoxides. On the other hand, compounds consisting of at least one sulfur and three oxygen atoms are predominantly assigned toward PAH- and PASH-sulfonates, confirming the desired sulfonation reaction. Products originating from the middle distillate have larger core structural motifs compared to products originating from the lighter distillation cut (e.g., sodium bituminosulfonate (SBS)), studied elsewhere.[15] We hypothesize that this molecular change, utilizing molecular weight and aromatic core size, will lead to more robust surfactant properties (increasing tenside character) following the typical apolar tail versus polar head chemistry. In the production process, the oil phase separation is incomplete or entirely missing after the sulfonation of the middle distillate in contrast to good phase separation after the sulfonation of the light distillate. This macroscopic observation from process engineering aids our surfactant hypothesis. Consequently, FT-ICR MS can describe complex reaction schemes and bulk properties previously revealed, e.g., for surfactant interfacial layer properties.[57]

As stated above, full sulfonation would cause an average shift of $n(SO_3)$. Since compounds with $S_{>0}O_{>2}$ were only found with negligible quantities in the distillate (Figure 3A), these constituents are considered as sulfonated species within the bituminosulfonates. As a result, we can estimate a sulfonation yield of approximately 36% in MABS and 27% in HABS based on the APPI FT-MS data based on the relative abundances. However, the average observed elemental shift of $S_{0.66}O_{0.83}$ also supports the hypothesis of complex side reactions. Another common side reaction in the exothermic process with sulfuric acid is oxidation. This effect is also observed by the compound class distribution (Figure 5A/B) featuring increased contribution of O_x, $S_xO_{<3}$ and $S_xO_{>3}$, the latter rationalized by a combination of sulfonation and oxidation. Since various sulfur-containing functionalities (e.g., sulfones, sulfoxides, and thioethers) have been identified as pharmacologically valuable in the treatment of various symptoms,[48,51] we recommend the consideration of the nonsulfonated and partially oxidized SCCs for future pharmacological studies besides the desired sulfonated constituents.

Complementary to the APPI results enabling a broad coverage of the chemical space, ESI selectively addressed the polar constituents. Thus, almost exclusively, sulfonates have been observed in ESI(−), attributing over 90% of the overall abundance to compound classes featuring SO_3 moieties (Figure 5B). GCxGC group-type analysis (Figure S13C) revealed distinct DBE-specific structural moieties for each compound class (e.g., thiophene- and benzothiophenesulfonates (DBE 3 and DBE 6, respectively) for CHO_3S_2). Therefore, the abundances of isomers found by GCxGC EI HR-ToF-MS analysis can be summed up to obtain data sets which are comparable to the direct infusion FT-ICR MS data,[31] allowing for an alignment of these data sets according to their assigned sum formulas. This further allows to tentatively transfer the structural elucidation achieved by the GCxGC analysis to the direct infusion ESI(−) data set. As a result, about 22% of the overall abundance of HABS detected in ESI(−) can be attributed toward sulfonated thiophenic and benzothiophenic core structural motifs. For MABS, the amount of sulfonated thiophenic and benzothiophenic backbones even makes up for one-third of the total abundance. Considerable amounts of other one- to three-ring PAH- and PASH-sulfonates were detected. The most abundant CH sulfonates (SO_3 class) were characterized as benzene-, indane-, and naphthalene-sulfonates, while bithiophene and thienobenzothiophene sulfonates were the most abundant core structural motifs for sulfonated S_2 compounds (S_3O_3 class). Both techniques revealed higher sulfonation yields for MABS, while HABS showed stronger tendencies toward oligomerization as well as slightly higher m/z ratios for each compound class (Figure S13A). This can be explained due to the fact that HABS is exclusively produced from the VDM, while both the vacuum distillate light (VDL) and the VDM are used for the MABS production. VDL consists of compounds with lower aromaticity and a lower degree of alkylation compared to VDM. Therefore, these compounds are more suitable for the sulfonation reaction, while the higher degree of alkylation in VDM favors steric hindrance, suppressing the sulfonation reaction, resulting in a lower sulfonation yield for HABS.

These core structural motifs correspond to some of the most abundant aromatic cores within the distillate, affirming these precursor compounds' sulfonation. However, indenic (DBE6) and phenylthiophenic (DBE7) cores as well as nonidentified

https://doi.org/10.1021/acs.analchem.4c01288
Anal. Chem. 2024, 96, 13050−13060

CHS_1 DBE4 species are significantly less frequently sulfonated in the product, although they exhibited abundances in the distillate comparable to those of the core structural motifs mentioned above. A similar finding was observed after sulfonation of the light distillate investigated elsewhere.[15] This finding points out the ability of the FT-ICR MS in conjunction with structural elucidation by GCxGC to find molecular preferences in the complex sulfonation reaction. Another critical aspect in sulfonation is the availability of free positions at the aromatic core targeted in the reaction. Sulfonation is impossible for aromatic compounds with alkylation at each position of the carbon backbone. Moreover, long alkylation chains may sterically hinder the sulfonation reaction. Hence, the alkylation pattern is a piece of intrinsically important information for generating the API in the studied production process. This assumption is supported by finding of generally lower alkylated compounds for the sulfonates, indicating higher sulfonation yields for less alkylated constituents. Finally, the GCxGC group-type analysis exclusively revealed nonsulfonated aliphatic and cyclic constituents, such as alkanes, cycloalkanes, and thiophanes. These compounds remain unchanged during the acidic and alkaline treatments, confirming that sulfonation reaction is solely possible at activated bonds (π electron contribution).[27,56]

To summarize, we present an adapted visualization plotting of the S/C ratio against m/z (Figures 6 and S19A). This concept enables the investigation of entire samples on a molecular level and tracing the described reaction pathways. Thereby, compounds with similar sulfur number group into tilted ellipses (Figure S19B). Homologous series along these tilted ellipses represent homologous series differing in their degree of alkylation (ΔCH_2) (Figure S19D). Horizontal lines represent hydrogen deficiencies between molecules, ultimately representing changes in unsaturation/aromaticity (Figure S19E). It is furthermore possible to distinguish between sulfonated and nonsulfonated compounds within the ellipses, since the sulfonic functional group leads to a higher m/z for the sulfonated compounds than for the nonsulfonated compounds with the same S/C ratio due to the oxygen atoms (Figure S19C). The effect caused by the sulfonation reaction is shown in Figure S19F, pointing out a switch between the ellipses due to the increasing sulfur content as well as the increasing m/z value. Fold change (FC)-based color coding enables molecular-level discrimination of two samples (Figure 6). Nonsulfonated monomeric constituents deplete after the sulfonation reaction, which can be found in the diagram by a negative FC for the lower part of each $S_{>0}$ ellipse (Figure 6A/B). In agreement, sulfonated compounds increase given the positive FC values for the upper part of each $S_{>0}$ ellipse. Generation of a noteworthy number of oligomeric SCCs causes an m/z shift larger than the mass of the sulfonate group. Comparison of the mixed and heavy sulfonate (Figure 6C) allows to observe higher sulfonation yield for the mixed product (negative FC for m/z < 400) and substantial oligomerization of the heavy product (positive FC for m/z > 400). These more pronounced oligomeric side reactions in the heavy product generated species with up to six organically bound sulfur atoms, rarely found in any other complex mixture analysis. The unique isotopic fine structure (IFS, Figure S16) with characteristic narrow mDa mass splits is directly accessible in rapid "dilute and shoot" analysis using the FT-ICR MS analyzer. As a result, this fingerprint comparison not only allows to characterize the samples on a molecular level but also allows the direct identification of educt−product relations and product−product discriminations along the multistep production process.

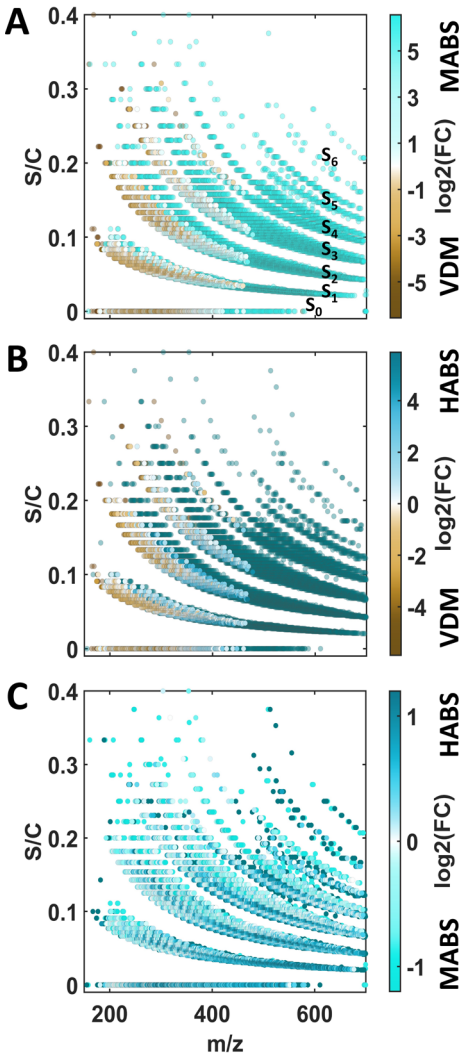

Figure 6. Modified van Krevelen diagram of APPI-based results showing the m/z ratio on the abscissa and the S/C ratio on the ordinate. (A) Shows the comparison of distillate (VDM) and mixed bituminosulfonate (MABS), (B) compares VDM and heavy bituminosulfonate (HABS), and (C) points out differences between MABS and HABS. The color coding describes the logarithmic fold changes (FC) between the samples. Negative values in (A) and (B) point out depleted compounds after sulfonation, while positive values highlight enriched compounds. In (C), negative values illustrate compounds that are enriched in MABS compared to HABS, while positive values point out depletion. Exemplarily, the number of organically bound sulfur atoms was assigned to the tilted ellipses in (A). These assignments are transferable to (B) and (C). Detailed interpretation guidance can be found in Figure S18.

4. CONCLUSIONS

In this study, we have successfully proven the applicability of ultrahigh-resolution mass spectrometry for chemically tracing the multistep manufacturing process of complex APIs. Specifically, ammonium bituminosulfonate APIs and their production process intermediates have been described at the molecular level. The combination of results from different

https://doi.org/10.1021/acs.analchem.4c01288
Anal. Chem. 2024, 96, 13050−13060

state-of-the-art analysis approaches enabled us to a) trace the entire production process, starting with solid bituminous schist via apolar liquid distillates to polar sulfonated APIs, b) identify structural moieties within the aromatic and heteroatom-rich mixture by data correlation with GCxGC HR-ToF-MS, and c) develop an understanding of transformation processes stepwise comparing the complex matrices.

Thermal analysis mass spectrometry of the source rock, mimicking reaction conditions of the large-scale industrial reactor, revealed high sulfur contribution in the evolved shale oil fraction. However, it could be shown that straightforward injection "dilute and shoot" analysis, avoiding cumbersome sample preparation protocols, resulted in in-depth insights into the complex chemistry of the sulfur-rich matrices in the following reaction steps. The superior resolving power and ppb-level mass accuracy of the FT-ICR MS analyzer allowed to distinguish mass signals with a mass difference of the mass of an electron (sub-mDa) and attribute elemental compositions with high confidence.

For the main processing step, the reaction of the complex shale oil distillate with sulfuric acid, high-resolution mass spectrometric profiling with two complementary ionization techniques (ESI/APPI), resulted in valuable information on the desired sulfonation ($+SO_3$) as well as side reactions, such as oligomerization (drastic increase in m/z) and oxidation ($+O_x$). Sulfur-containing functionalities described in the literature as pharmacologically active could be identified. Moreover, hypotheses and estimates on the structure-dependent sulfonation yield, strongly linked to steric hindrance by the degree of alkylation, could be concluded.

The study proves that ultrahigh-resolution mass spectrometry delivers valuable molecular information on complex APIs. The presented approach allows differentiation between manufacturing process-related chemical alterations as well as different products originating from the same source rock. Hence, a high potential for source-related chemical profiling is given. We believe that this approach is essential for the detailed chemical characterization of complex pharmaceuticals in general, as chemical insights may help improve manufacturing processes and pharmacological efficacy. Routine methodologies established for classical pharmacological analysis would not have been suitable to cope with the high complexity. However, the in-depth chemical information enables the development of routine analysis methods for quality assurance without the need of reaching full structural elucidation routinely. Consequently, future studies will focus on further developing chromatographic or tandem mass spectrometric analysis protocols in the complex API framework. Moreover, we recommend utilizing this chemical information in future work to test for the pharmacological properties of specific compound classes. Combining chemical and pharmacological information will help adjusting the manufacturing process to promote specific therapeutic properties.

■ ASSOCIATED CONTENT

Data Availability Statement

All FT-ICR mass spectra files and assigned elemental compositions are publicly available via the Open Science Framework, DOI: 10.17605/OSF.IO/AM8TV.

Supporting Information

The Supporting Information is available free of charge at https://pubs.acs.org/doi/10.1021/acs.analchem.4c01288.

Details on the temperature programs for thermogravimetric analysis (Table S1); complete flowchart of the manufacturing process (Figure S1); compound class distribution of the thermogravimetric high-resolution mass spectrometric analysis (Figure S2; time-resolved total ion current for TGA APPI-FT-ICR MS analysis including time- and temperature-related mass spectra (Figure S3); zoom-in for m/z 400 for thermal analysis mass spectrometry via 7 T FT-ICR MS (Figure S4); zoom-in for SCO at m/z 313 for 21 T direct infusion APPI FT-ICR MS (Figure S5); GCxGC contour plots of the four matrices investigated (Figure S5); exemplary contour plots showing the empirically evaluated elution windows for the ammonium bituminosulfonates (Figure S7); calculated relative and intensity-weighted elemental composition of SCO, VDM, MABS, and HABS (Figure S8); overview of bulk parameters exemplarily depicted from direct infusion APPI FT-ICR MS measurements (Figure S9); APPI data-based isoabundance DBE vs #C plots (Figure S10); zoom-in for HABS at m/z 313 for 21 T direct infusion APPI FT-ICR MS (Figure S11); Venn diagrams comparing the APPI results of the different matrices as well as comparing the different ionization techniques for mixed ammonium bituminosulfonate (Figure S12); overview of bulk parameters exemplarily depicted from direct infusion APPI FT-ICR MS measurements of MABS and HABS (Figure S13); overview of the elemental distributions by the number of assigned sum formulas identified by APPI (Figure S14); ESI(−) data-based isoabundance DBE vs #C plots (Figure S15); calculated isotopic fine structure (IFS) for sulfur moieties with one to six sulfur atoms (Figure S16); Kendrick plots showing the CH_2−related Kendrick mass defect and the SO_3-related Kendrick mass defect plotted for all matrices investigated (Figure S17); process-related Kendrick plots illustrating the comparison of VDM to both bituminosulfonates utilizing fold change-based color coding (Figure S18); and modified van Krevelen diagram of APPI data-based results showing the m/z ratio on the abscissa and the S/C ratio on the ordinate (Figure S19) (PDF)

■ AUTHOR INFORMATION

Corresponding Author

Christopher P. Rüger − *Chair of Analytical Chemistry/Joint Mass Spectrometry Centre (JMSC), University of Rostock, 18059 Rostock, Germany; Department Life, Light and Matter (LLM), University of Rostock, 18059 Rostock, Germany; International Joint Laboratory−iC2MC: Complex Matrices Molecular Characterization, 76700 Harfleur, France;* orcid.org/0000-0001-9634-9239; Email: christopher.rueger@uni-rostock.de

Authors

Ole Tiemann − *Chair of Analytical Chemistry/Joint Mass Spectrometry Centre (JMSC), University of Rostock, 18059 Rostock, Germany; Department Life, Light and Matter (LLM), University of Rostock, 18059 Rostock, Germany*

Lukas Schwalb − *Chair of Analytical Chemistry/Joint Mass Spectrometry Centre (JMSC), University of Rostock, 18059 Rostock, Germany; Helmholtz Zentrum München GmbH, German Research Center for Environmental Health, 85764 Neuherberg, Germany; Cooperation group "Comprehensive*

Molecular Analytics" (CMA), Joint Mass Spectrometry Centre (JMSC), 81379 Munich, Germany

Martha L. Chacón-Patiño − *International Joint Laboratory−iC2MC: Complex Matrices Molecular Characterization, 76700 Harfleur, France; Ion Cyclotron Resonance Program, National High Magnetic Field Laboratory, Florida State University, Tallahassee, Florida 32310, United States;* orcid.org/0000-0002-7273-5343

Thomas Gröger − *Chair of Analytical Chemistry/Joint Mass Spectrometry Centre (JMSC), University of Rostock, 18059 Rostock, Germany; Helmholtz Zentrum München GmbH, German Research Center for Environmental Health, 85764 Neuherberg, Germany; Cooperation group "Comprehensive Molecular Analytics" (CMA), Joint Mass Spectrometry Centre (JMSC), 81379 Munich, Germany;* orcid.org/0000-0001-9882-7388

Ralf Zimmermann − *Chair of Analytical Chemistry/Joint Mass Spectrometry Centre (JMSC), University of Rostock, 18059 Rostock, Germany; Department Life, Light and Matter (LLM), University of Rostock, 18059 Rostock, Germany; Helmholtz Zentrum München GmbH, German Research Center for Environmental Health, 85764 Neuherberg, Germany; Cooperation group "Comprehensive Molecular Analytics" (CMA), Joint Mass Spectrometry Centre (JMSC), 81379 Munich, Germany*

Complete contact information is available at: https://pubs.acs.org/10.1021/acs.analchem.4c01288

Author Contributions

O.T.: data curation, formal analysis, investigation, methodology, visualization, and writing − original draft preparation; C.P.R.: conceptualization, funding acquisition, methodology, project administration, software, supervision, visualization, and writing − original draft preparation; M.L.C.P.: data curation, formal analysis, investigation, and methodology; L.S.: formal analysis, investigation, methodology, and writing − review and editing; T.G.: funding acquisition, project administration, supervision, writing − review and editing; and R.Z.: funding acquisition, project administration, resources.

Funding

The study was funded by Ichthyol-Gesellschaft Cordes, Hermanni & Co (GmbH &Co.) KG.

Notes

The authors declare no competing financial interest.

■ ACKNOWLEDGMENTS

We thank Dr. Guido Gayko and the Ichthyol-Gesellschaft for providing the sample material and the information on the production process of the bituminosulfonates. Part of this work was performed at the National High Magnetic Field Laboratory, MagLab, located in Tallahassee, Florida, USA, which is supported by the NSF Division of Materials and Chemistry Research through 16-44779/21-28556 and the State of Florida. The authors thank the DFG for funding of the Bruker FT-ICR MS (INST 264/56).

■ REFERENCES

(1) Lee Ventola, C. *Pharm. Ther.* **2015**, *40* (4), 277−283.
(2) Gawrońska, M.; Kowalik, M.; Makowski, M. *TrAC Trends in Analytical Chemistry* **2022**, *155*, No. 116691.
(3) Rosalia, M.; Chiesa, E.; Tottoli, E. M.; Dorati, R.; Genta, I.; Conti, V.; Pisani, S. *Int. J. Mol. Sci.* **2022**, *23* (22), 14080.
(4) Europäisches Arzneibuch 11. Ausgabe, 1. In *Nachtrag: Amtliche deutsche Ausgabe (Ph. Eur. 11.1)*, 1. Auflage; Deutscher Apotheker Verlag, 2024.
(5) International Council for Harmonisation of technical Requirements for Pharmaceuticals for Human Use (ICH). Quality System (Q10). In *ICH Quality Guidelines*, 2008. https://database.ich.org/sites/default/files/Q10%20Guideline.pdf.
(6) International Council for Harmonisation of technical Requirements for Pharmaceuticals for Human Use (ICH). *Continuous Manufacturing of Drug Substances and Drug Products Q13*, 2022. https://database.ich.org/sites/default/files/ICH_Q13_Step4_Guideline_2022_1116.pdf.
(7) International Council for Harmonisation of technical Requirements for Pharmaceuticals for Human Use (ICH). *Validation of Analytical Procedures Q2(R2)*, 2023. https://database.ich.org/sites/default/files/ICH_Q2%28R2%29_Guideline_2023_1130.pdf.
(8) Crommelin, D. J. A.; de Vlieger, J. S. B.; Weinstein, V.; Mühlebach, S.; Shah, V. P.; Schellekens, H. *AAPS journal* **2014**, *16* (1), 11−14.
(9) Klein, K.; Borchard, G.; Shah, V. P.; Flühmann, B.; McNeil, S. E.; de Vlieger, J. S. B. *Ann. N.Y. Acad. Sci.* **2021**, *1502* (1), 5−13.
(10) Klein, K.; Stolk, P.; de Bruin, M. L.; Leufkens, H. G. M.; Crommelin, D. J. A.; de Vlieger, J. S. B. *European Journal of Pharmaceutical Sciences* **2019**, *133*, 228−235.
(11) Schellekens, H.; Klinger, E.; Mühlebach, S.; Brin, J.-F.; Storm, G.; Crommelin, D. J. A. *Regul. Toxicol. Pharmacol.* **2011**, *59*, 176−183.
(12) Gabizon, A.; Shmeeda, H.; Barenholz, Y. *Clinical Pharmacokinetics* **2003**, *42*, 419−436.
(13) Toblli, J. E.; Cao, G.; Oliveri, L.; Angerosa, M. *Therapeutics for States of Dificiency* **2009**, *59* (4), 176−190.
(14) Melamed-Gal, S.; Loupe, P.; Timan, B.; Weinstein, V.; Kolitz, S.; Zhang, J.; Funt, J.; Komlosh, A.; Ashkenazi, N.; Bar-Ilan, O.; Konya, A.; Beriozkin, O.; Laifenfeld, D.; Hasson, T.; Krispin, R.; Molotsky, T.; Papir, G.; Sulimani, L.; Zeskind, B.; Liu, P.; Nock, S.; Hayden, M. R.; Gilbert, A.; Grossman, I. *eNeurologicalSci.* **2018**, *12*, 19−30.
(15) Schwalb, L.; Tiemann, O.; Käfer, U.; Gröger, T.; Rüger, C. P.; Gayko, G.; Zimmermann, R. *Anal. Bioanal. Chem.* **2023**, *415*, 2471.
(16) Fink, S.; Sethmann, A.; Hipler, U.-C.; Wiegand, C. *European Journal of Pharmaceutical Sciences* **2022**, *172*, No. 106152.
(17) Gayko, G.; Cholcha, W.; Kietzmann, M. *Berl. Munch. Tierarztl. Wochenschr.* **2000**, *113* (10), 368−373.
(18) Korting, H. C.; Schöllmann, C.; Cholcha, W.; Wolff, L. *Journal of the European Academy of Dermatology and Venereology: JEADV* **2010**, *24* (10), 1176−1182.
(19) Unna, P. G. IV. Ichthyol. In *Monatshefte für Praktische Dermatologie*; Leopold Voss: Leipzig, Hamburg, 1882; pp. 328-333.
(20) Nilssen, E.; Wormald, P. J.; Oliver, S. *Journal of Laryngology and Otology* **1996**, *110*, 319−321.
(21) Idelevich, E. A.; Becker, K. *Microbial Drug Resistance* **2020**, *26* (11), 1405−1409.
(22) Ahmed, K.; Roberts, M. L.; Mannion, P. T. *Clinical Otolaryngology & Allied Sciences* **1995**, *20*, 201−203.
(23) Pailer, M.; Simonitsch, E. *Monatsh. Chem.* **1967**, *98*, 1477−1491.
(24) Pailer, M.; Begutter, H. *Monatshefte der Chemie* **1973**, *104*, 297−311.
(25) Koch, J.; Moser, R.; Demel, J. *Archiv der Pharmazie* **1985**, *318*, 198−206.
(26) Feng, Z.; Cui, M.; Liu, J.; Song, Y.; Li, J. Q. *Asian J. Chem.* **2014**, *26* (20), 6722−6726.
(27) Li, S.; Wu, J.; Zhang, W.; Jiang, Y.; Hu, M.; Chung, K. H.; Shi, Q. *Anal. Bioanal. Chem.* **2023**, *415* (10), 1889−1896.
(28) Panchal, K.; Katke, S.; Dash, S. K.; Gaur, A.; Shinde, A.; Saha, N.; Mehra, N. K.; Chaurasiya, A. *Drug delivery and translational research* **2023**, *13* (2), 433−472.
(29) Kleindl, P. A.; Xiong, J.; Hewarathna, A.; Mozziconacci, O.; Nariya, M. K.; Fisher, A. C.; Deeds, E. J.; Joshi, S. B.; Middaugh, C.

R.; Schöneich, C.; Volkin, D. B.; Forrest, M. L. *Journal of pharmaceutical sciences* **2017**, *106* (11), 3242−3256.
(30) Davani, B. *Pharmaceutical Analysis for Small Molecules*; John Wiley & Sons Incorporated, 2017.
(31) Schwalb, L.; Tiemann, O.; Käfer, U.; Rüger, C. P.; Gröger, T.; Zimmermann, R. *Anal. Bioanal. Chem.* **2024**, *416*, 1033.
(32) Deschamps, E.; Calabrese, V.; Schmitz, I.; Hubert-Roux, M.; Castagnos, D.; Afonso, C. *Molecules* **2023**, *28* (5), 2061.
(33) Holt, A. D.; Kellerman, A. M.; Battin, T. I.; McKenna, A. M.; Hood, E.; Andino, P.; Crespo-Pérez, V.; Peter, H.; Schön, M.; de Staercke, V.; Styllas, M.; Tolosano, M.; Spencer, R. G. M. *JGR Biogeosci.* **2023**, *128* (5), No. e2022JG007188, DOI: 10.1029/2022JG007188.
(34) Gray, M. R.; Chacón-Patiño, M. L.; Rodgers, R. P. *Energy Fuels* **2022**, *36* (8), 4370−4380.
(35) Popovic, Z.; Anderson, L. C.; Zhang, X.; Butcher, D. S.; Blakney, G. T.; Zubarev, R. A.; Marshall, A. G. *J. Am. Soc. Mass Spectrom.* **2023**, *34* (2), 137−144.
(36) Chacón-Patiño, M. L.; Moulian, R.; Barrère-Mangote, C.; Putman, J. C.; Weisbrod, C. R.; Blakney, G. T.; Bouyssiere, B.; Rodgers, R. P.; Giusti, P. *Energy Fuels* **2020**, *34* (12), 16158−16172.
(37) Tsybin, Y. O.; Nagornov, K. O.; Kozhinov, A. N. Advanced fundamentals in Fourier transform mass spectrometry. In *Fundamentals and Applications of Fourier Transform Mass Spectrometry*, 1st ed.; Schmitt-Kopplin, P.; Kanawati, B., Eds.; Elsevier, 2019; pp. 113−132.
(38) Wootton, C. A.; Lam, Y. P. Y.; Willetts, M.; van Agthoven, M. A.; Barrow, M. P.; Sadler, P. J.; O'Connor, P. B. *Analyst* **2017**, *142* (11), 2029−2037.
(39) Wootton, C. A.; Sanchez-Cano, C.; Liu, H.-K.; Barrow, M. P.; Sadler, P. J.; O'Connor, P. B. *Dalton transactions (Cambridge, England: 2003)* **2015**, *44* (8), 3624−3632.
(40) Rüger, C. P.; Grimmer, C.; Sklorz, M.; Neumann, A.; Streibel, T.; Zimmermann, R. *Energy Fuels* **2018**, *32* (3), 2699−2711.
(41) Rüger, C. P.; Miersch, T.; Schwemer, T.; Sklorz, M.; Zimmermann, R. *Analytical chemistry* **2015**, *87* (13), 6493−6499.
(42) Neumann, A.; Käfer, U.; Gröger, T.; Wilharm, T.; Zimmermann, R.; Rüger, C. P. *Energy Fuels* **2020**, *34*, 10641.
(43) Zherebker, A.; Kostyukevich, Y.; Volkov, D. S.; Chumakov, R. G.; Friederici, L.; Rüger, C. P.; Kononikhin, A.; Kharybin, O.; Korochantsev, A.; Zimmermann, R.; Perminova, I. V.; Nikolaev, E. *Sci. Rep.* **2021**, *11* (1), 7410.
(44) Rüger, C. P.; Schwemer, T.; Sklorz, M.; O'Connor, P. B.; Barrow, M. P.; Zimmermann, R. *European journal of mass spectrometry (Chichester, England)* **2017**, *23* (1), 28−39.
(45) Hendrickson, C. L.; Quinn, J. P.; Kaiser, N. K.; Smith, D. F.; Blakney, G. T.; Chen, T.; Marshall, A. G.; Weisbrod, C. R.; Beu, S. C. *J. Am. Soc. Mass Spectrom.* **2015**, *26* (9), 1626−1632.
(46) Savory, J. J.; Kaiser, N. K.; McKenna, A. M.; Xian, F.; Blakney, G. T.; Rodgers, R. P.; Hendrickson, C. L.; Marshall, A. G. *Analytical chemistry* **2011**, *83* (5), 1732−1736.
(47) Amer, M. W.; Aljariri Alhesan, J. S.; Marshall, M.; Awwad, A. M.; Al-Ayed, O. S. *Journal of Analytical and Applied Pyrolysis* **2019**, *140*, 219−226.
(48) Guo, F.-W.; Zhang, Q.; Gu, Y.-C.; Shao, C.-L. *Curr. Opin. Chem. Biol.* **2023**, *75*, No. 102330.
(49) Bae, E.; Na, J.-G.; Chung, S. H.; Kim, H. S.; Kim, S. *Energy Fuels* **2010**, *24* (4), 2563−2569.
(50) Boduszynski, M. M. *Energy Fuels* **1987**, *1* (1), 2−11.
(51) Mustafa, M.; Winum, J.-Y. *Expert opinion on drug discovery* **2022**, *17* (5), 501−512.
(52) Chacón-Patiño, M. L.; Gray, M. R.; Ruger, C.; Smith, D. F.; Glattke, T. J.; Niles, S. F.; Neumann, A.; Weisbrod, C. R.; Yen, A.; McKenna, A. M.; Giusti, P.; Bouyssiere, B.; Barrere-Mangote, C.; Yarranton, H.; Hendrickson, C. L.; Marshall, A. G.; Rodgers, R. P. *Energy Fuels* **2021**, *35*, 16335−16376.
(53) Chacón-Patiño, M. L.; Rowland, S. M.; Rodgers, R. P. The Compositional and Structural Continuum of Petroleum from Light Distillates to Asphaltenes: The Boduszynski Continuum Theory As Revealedby FT-ICR Mass Spectrometry. In *The Boduszynski Continuum: Contributions to the Understanding of the Molecular Composition of Petroleum*; American Chemical Society: 2008, 113−171 .
(54) McKenna, A. M.; Purcell, J. M.; Rodgers, R. P.; Marshall, A. G. *Energy Fuels* **2010**, *24*, 2929−2938.
(55) Smith, D. F.; Rahimi, P.; Teclemariam, A.; Rodgers, R. P.; Marshall, A. G. *Energy Fuels* **2008**, *22* (5), 3118−3125.
(56) Katritzky, A. R.; Kim, M. S.; Fedoseyenko, D.; Widyan, K.; Siskin, M.; Francisco, M. *Tetrahedron* **2009**, *65*, 1111−1114.
(57) Niles, S. F.; Chacon-Patino, M. L.; Chen, H.; Marshall, A. G.; Rodgers, R. P. *Energy Fuels* **2021**, *35*, 18153−18162.

https://doi.org/10.1021/acs.analchem.4c01288
Anal. Chem. 2024, 96, 13050−13060